

Time-Domain Extraction of Broad-Band Sources by  
Tikhonov-Phillips Regularization of Triangular Toeplitz  
Kernels\*Jacob Roginsky<sup>†</sup>G. W. Stewart<sup>‡</sup>

August 1995

## ABSTRACT

Single receiver source deconvolution in a shallow water environment is an ill-posed problem whose difficulty is compounded by the multipath nature of the propagation operator. If only sources that are quiescent prior to some initial time  $t_0$  are considered, the result of discretizing the problem in the time domain is an ill-conditioned triangular Toeplitz system. In this paper we show how an algorithm of Eldén can be used to implement Tikhonov-Phillips regularization for this system. Unlike the multichannel deconvolution techniques used in underwater acoustics, this method can extract source signatures using the outputs of a single sensor. In addition, when the propagation is multipath and source signature extraction is performed as part of an optimization procedure for environmental inversion, we can work with shorter time windows so that the process becomes computationally more efficient than frequency domain deconvolution. A number of examples of the use of the Tikhonov-Phillips regularization method for source series extraction are provided.

---

\*This report is available by anonymous ftp from `thales.cs.umd.edu` in the directory `pub/reports`.

<sup>†</sup>University of Maryland, College Park, MD 20742

<sup>‡</sup>Department of Computer Science and Institute for Advanced Computer Studies, University

# Time-Domain Extraction of Broad-Band Sources by Tikhonov–Phillips Regularization of Triangular Toeplitz Kernels

Jacob Roginsky, Naval Research Laboratory, Washington DC 20375-5350

G. W. Stewart, University of Maryland, College Park, MD 20742

## ABSTRACT

Single receiver source deconvolution in a shallow water environment is an ill-posed problem whose difficulty is compounded by the multipath nature of the propagation operator. If only sources that are quiescent prior to some initial time  $t_0$  are considered, the result of discretizing the problem in the time domain is an ill-conditioned triangular Toeplitz system. In this paper we show how an algorithm of Eldén can be used to implement Tikhonov–Phillips regularization for this system. Unlike the multichannel deconvolution techniques used in underwater acoustics, this method can extract source signatures using the outputs of a single sensor. In addition, when the propagation is multipath and source signature extraction is performed as part of an optimization procedure for environmental inversion, we can work with shorter time windows so that the process becomes computationally more efficient than frequency domain deconvolution. A number of examples of the use of the Tikhonov–Phillips regularization method for source series extraction are provided.

(PACS) Subject Classification numbers: 43.30.Pc, 43.60.Pt

## 1 Introduction

The problem of determining the input function of a linear integral equation from its output function arises frequently in physics and engineering. When the equation in question is a Fredholm equation

$$y(t) = \int_a^b k(t, \tau)x(\tau)d\tau, \quad t \in [a, b],$$

or a Volterra equation

$$y(t) = \int_a^t k(t, \tau)x(\tau)d\tau, \quad t \in [a, b]$$

---

of Maryland, College Park, MD 20742.

with a kernel of the form

$$k(t, \tau) = P(t - \tau)$$

the process is called deconvolution because the integrals are convolutions of the kernel with the operand.

Examples of such problems can be found in geophysics, applied optics, communication theory, and applied electromagnetics (see [16] for further references), as well as thermodynamics [7] and underwater acoustics [8, 11, 12]. In linear acoustics the problem is usually that of determining the source time series based on a known medium impulse response and a noisy receiver time series.

The problem treated in this paper is the deconvolution of a signal satisfying the Volterra equation

$$r(t) = \int_0^t P(t - \tau)s(\tau) d\tau + n(t), \quad 0 \leq t \leq T. \quad (1)$$

Here  $r(t)$  is the receiver amplitude at time  $t$ ,  $P(t - \tau)$  is the response of the receiver at time  $t$  to a unit source pulse at time  $\tau$ , and  $s(\tau)$  is the amplitude of the source at time  $\tau$ . The function  $n(t)$  represents noise, which for simplicity we assume to be white. We also assume that the origin has been adjusted to take into account the propagation time for the signal to arrive at the receiver.

In some cases the discretization of equation (1) produces relatively well-conditioned linear systems of equations [1]. If  $T$  is greater than the impulse-response dissipation time and all of the source response is collected, one benefits greatly from considering the problem in the frequency domain, where the propagator's matrix representation is diagonal. Apart from the computational simplicity, an important benefit of such an approach is that any ill-conditioning of the operator is manifested by small diagonal entries in the matrix.

Whenever  $P$  is relatively smooth or  $P(0)$  is very small compared to the root mean square of  $P$ , as is the case in most time series deconvolution problems [13], the resulting system will generally be quite ill-conditioned. However, the causes of ill-conditioning are different for the two cases.

1. If the kernel is smooth it will map highly oscillatory functions into small functions as the positive and negative parts of the oscillations cancel one another. To look at it conversely, there are "bad" functions that get mapped by the inverse operator into large oscillatory functions. If the output function were free of noise and our inversion techniques free of numerical errors, this would not be a problem. But both noise and rounding errors introduce

components along the bad functions, which in the subsequent inversion grow and swamp the input signal.

2. Because the signal follows multiple paths it does not arrive at the receiver all at once but builds up gradually. This implies that  $P(t)$  is small when  $t = 0$  and increases slowly. In particular, the operator effectively annihilates signals that are zero except at the end of the sampling window. The discrete analogue is a triangular matrix with small elements on and near its principal diagonal.

There are a number of techniques that stabilize the source deconvolution process for a single receiver. A good survey of those techniques is given by Hanke and Hansen [10]. Two popular methods are based on techniques of projection and regularization. A bidiagonalization-regularization technique [13] is a combination of the two. The singular value decomposition can be used to implement a projection technique that is very reliable [2]. But it is an  $O(n^3)$  process in the number of matrix elements and is too slow for some applications with large  $n$ . There are iterative methods to regularize problems, many of which show promise [10].

Statistical techniques of deconvolution have been applied by geophysicists and marine seismologists for quite some time [18, 6]. A statistical technique of multi-channel deconvolution was recently introduced into underwater acoustics [5, 11]. Berenstein and Patrick [4] showed that the ill-posed deconvolution problem can be transformed into a well-posed one by introduction of multi-sensor processing.

These statistical deconvolutions are performed in the frequency domain. Prior to the deconvolution the Green's functions for the sensors are computed using the wave equation. However, for a multipath environment the computation time can become a serious concern if the task calls for numerous propagations and deconvolutions, as, for example, in environmental inversions with unknown sources. In this case time domain computations with shorter time windows that take advantage of the Toeplitz structure of the operator become an attractive alternative.

For our problem the environment is a stratified shallow water column overlying a simple bottom. Propagations are very short range ( $> 300\text{m}$ ). The wave model of choice is the Fast Field Program [15], which takes advantage of the medium stratification. The computational cost of running the model is roughly proportional to the square of the propagation time. Figure 1 shows how the particular choice of the source and receiver time windows for the deconvolution results in a lower triangular Toeplitz system of equations. The system is ill-conditioned, and it will be treated by the Tikhonov–Phillips regularization method

[14, 17]. A natural advantage of Tikhonov–Phillips regularization is that, unlike multichannel deconvolution methods, it can be applied in situations where only one sensor is available. Although conventional implementations of this method require  $O(n^3)$  work, we will use an algorithm of Eldén [9] that takes advantage of the triangular Toeplitz structure of  $P$  to reduce the time to  $O(n^2)$ , a time much shorter than the times for broad-band wave-mechanical computations.

In the next section we will introduce the discretization and describe Tikhonov–Phillips regularization. In §3 we will sketch Eldén’s algorithm. Some numerical examples will be presented in the subsequent section followed by conclusions and suggestions for future work.

## 2 Tikhonov–Phillips Regularization of the Discrete Problem

To discretize (1), divide the interval  $[0, T]$  by equally spaced points  $t_i$  ( $i = 0, \dots, n$ ) and assume that the signal has been sampled by the receiver at the times  $t_i$  to give values  $r_i$ . Let  $s_i$  be the corresponding source values. If for  $t = t_i$  we approximate the integrand in (1) by the step function whose values in  $[t_j, t_{j+1})$  are  $P(t_i - t_j)s_j$ , and introduce the time discretization step  $h = T/n$ , we obtain the system of equations

$$r_i = h \sum_{j=0}^n P(t_i - t_j)s_j, \quad j = 0, 1, \dots, n.$$

In terms of matrices and vectors, if we let  $P$  be the matrix whose  $(i, j)$  element is

$$p_{i-j} = \begin{cases} hP(t_i - t_j) & \text{if } i \geq j, \\ 0 & \text{if } i < j, \end{cases}$$

and set

$$r = \begin{pmatrix} r_0 \\ r_1 \\ \vdots \\ r_n \end{pmatrix} \quad \text{and} \quad s = \begin{pmatrix} s_0 \\ s_1 \\ \vdots \\ s_n \end{pmatrix},$$

then

$$Ps = r. \tag{2}$$

The matrix  $P$  is a lower triangular Toeplitz matrix whose elements are constant along its diagonals. It is illustrated below for the case  $n = 4$ :

$$P = \begin{pmatrix} p_0 & 0 & 0 & 0 & 0 \\ p_1 & p_0 & 0 & 0 & 0 \\ p_2 & p_1 & p_0 & 0 & 0 \\ p_3 & p_2 & p_1 & p_0 & 0 \\ p_4 & p_3 & p_2 & p_1 & p_0 \end{pmatrix}.$$

As we have noted, the matrix  $P$  will be ill-conditioned, and the attempt to solve (2) by conventional techniques will give meaningless results. The idea behind Tikhonov–Phillips regularization is to restrict the solution  $s$  so that a prescribed linear constraint function  $Cs$  is bounded. Since the constraint may make it impossible to solve (2) exactly, we solve it in a least squares sense. Thus we solve the problem

$$\begin{aligned} & \text{minimize} && \|r - Ps\|, \\ & \text{subject to} && \|Cs\| \leq \alpha, \end{aligned} \tag{3}$$

where  $\|\cdot\|$  is the usual Euclidean norm and  $\alpha$  is a parameter whose size controls the amount of regularization. From the theory of Lagrange multipliers, we find that for each  $\alpha$  there is a  $\lambda$  such that the solution of the problem

$$\text{minimize} \quad \left\| \begin{pmatrix} r \\ 0 \end{pmatrix} - \begin{pmatrix} Ps \\ \lambda Cs \end{pmatrix} \right\| \tag{4}$$

is also the solution of (3). This form of the method is better suited to numerical computation, since (4) is a linear least squares problem.

The operator  $C$  is usually chosen to constrain the size of the function or its derivatives. For example, if we take  $C = I$ , the the constraint in (3) becomes  $\|s\| \leq \alpha$  — a constraint on the size of the solution. If

$$C = \begin{pmatrix} 1 & 0 & 0 & 0 & 0 \\ -1 & 1 & 0 & 0 & 0 \\ 0 & -1 & 1 & 0 & 0 \\ 0 & 0 & -1 & 1 & 0 \\ 0 & 0 & 0 & -1 & 1 \end{pmatrix} \quad \text{or} \quad C = \begin{pmatrix} -1 & 0 & 0 & 0 & 0 \\ 2 & -1 & 0 & 0 & 0 \\ -1 & 2 & -1 & 0 & 0 \\ 0 & -1 & 2 & -1 & 0 \\ 0 & 0 & -1 & 2 & -1 \end{pmatrix}$$

then the constraint is effectively on the first or second derivative, since the rows of  $C$  (excepting the initial rows) consist of the coefficients of first or second difference quotients.

### 3 Eldén's Algorithm

For any value of  $\lambda$  the least squares problem (4) can be solved by standard techniques. Unfortunately, these techniques take  $O(n^3)$  time. However, if the constraint matrix  $C$  is itself Toeplitz and lower triangular, as it is in the three examples above, we can use an elegant algorithm of Eldén that takes only  $O(n^2)$  time. Eldén's description of his algorithm is directed toward numerical analysts and assumes a great deal of background. It is therefore appropriate to give a new presentation of the algorithm. For brevity in the following exposition, we will suppose that the Lagrange multiplier  $\lambda$  has been absorbed into the matrix  $C$ .

The derivation consists of three distinct parts: the solution of least squares problems by orthogonal triangularization, plane rotations, and the algorithm itself. We will treat each in turn.

To solve least squares problems by orthogonal triangularization we assume we have at hand an orthogonal matrix  $Q$  such that

$$Q^T \begin{pmatrix} P \\ C \end{pmatrix} = \begin{pmatrix} L \\ 0 \end{pmatrix}, \quad (5)$$

where  $L$  is lower triangular. Since the Euclidean norm is invariant under orthogonal transformations, we have that the residual sum of squares (RSS) satisfies

$$\text{RSS} \equiv \left\| \begin{pmatrix} r \\ 0 \end{pmatrix} - \begin{pmatrix} P_s \\ C_s \end{pmatrix} \right\|^2 = \left\| Q^T \begin{pmatrix} r \\ 0 \end{pmatrix} - Q^T \begin{pmatrix} P_s \\ C_s \end{pmatrix} \right\|^2.$$

Hence if we partition

$$Q^T \begin{pmatrix} r \\ 0 \end{pmatrix} = \begin{pmatrix} u \\ g \end{pmatrix}, \quad (6)$$

we have

$$\text{RSS} = \left\| \begin{pmatrix} u - Ls \\ g \end{pmatrix} \right\|^2 = \|u - Ls\|^2 + \|g\|^2.$$

The second term on the right-hand side of this expression is independent of  $s$ . Consequently RSS will be minimized when  $s$  is chosen to minimize the first term. Since this term is nonnegative, it will be minimized when  $u - Ls = 0$ . Or  $Ls = u$ . This is a triangular system that can be solved by forward substitution in  $O(n^2)$  operations.

At this point the remaining problem is to determine  $Q$  and  $L$ . The computational tool for this is the plane rotations. A plane rotation is determined by two

numbers  $c$  and  $s$  satisfying  $c^2 + s^2 = 1$ . It acts in the  $(i, j)$ -plane if, when it is applied to a matrix  $A$ , it changes the  $i$ th and  $j$ th rows as follows:

$$\begin{pmatrix} a_i^T \\ a_j^T \end{pmatrix} \leftarrow \begin{pmatrix} c & s \\ -s & c \end{pmatrix} \begin{pmatrix} a_i^T \\ a_j^T \end{pmatrix}. \quad (7)$$

This transformation of  $A$  is orthogonal, since the  $2 \times 2$  matrix that transforms the two rows of  $A$  is orthogonal.

The value of plane rotations is that they can be used to introduce zeros selectively into a matrix. If, for example, in (7) we set

$$c = \frac{a_{ik}}{\sqrt{a_{ik}^2 + a_{jk}^2}} \quad \text{and} \quad s = \frac{a_{jk}}{\sqrt{a_{ik}^2 + a_{jk}^2}}$$

then it is easily verified that

$$\begin{pmatrix} c & s \\ -s & c \end{pmatrix} \begin{pmatrix} a_{ik} \\ a_{jk} \end{pmatrix} = \begin{pmatrix} \sqrt{a_{ik}^2 + a_{jk}^2} \\ 0 \end{pmatrix}.$$

Thus for this particular choice of  $c$  and  $s$ , the transformation (7) puts a zero in the  $(j, k)$ -element of  $A$ .

We are now in a position to describe Eldén's reduction. It is sufficiently well illustrated for the case  $n = 3$ .

Since the transformations that are applied to  $P$  and  $C$  in (5) must be applied to the vector  $r$  and its companion zero in (6), it will be convenient to arrange them all in the same matrix:

$$\begin{pmatrix} p_0 & 0 & 0 & 0 & r_0 \\ p_1 & p_0 & 0 & 0 & r_1 \\ p_2 & p_1 & p_0 & 0 & r_2 \\ p_3 & p_2 & p_1 & p_0 & r_3 \\ c_0 & 0 & 0 & 0 & g_0 \\ c_1 & c_0 & 0 & 0 & g_1 \\ c_2 & c_1 & c_0 & 0 & g_2 \\ c_3 & c_2 & c_1 & c_0 & g_3 \end{pmatrix}.$$

Here the  $g_i$  are initially zero. We now apply a rotation in the  $(4, 8)$ -plane to



annihilate  $c_0$ . The result is a matrix of the form

$$\begin{pmatrix} p_0 & 0 & 0 & 0 & r_0 \\ p_1 & p_0 & 0 & 0 & r_1 \\ p_2 & p_1 & p_0 & 0 & r_2 \\ p'_3 & p'_2 & p'_1 & p'_0 & r'_3 \\ c_0 & 0 & 0 & 0 & g_0 \\ c_1 & c_0 & 0 & 0 & g_1 \\ c_2 & c_1 & c_0 & 0 & g_2 \\ c'_3 & c'_2 & c'_1 & 0 & g'_3 \end{pmatrix},$$

in which the primes indicate altered values. The application of this plane rotation takes only  $O(n)$  operations.

The key to the algorithm is based on the observation that if we apply the same rotations in the (3, 7)-, (2, 6)-, and (1, 5)-planes, we get the matrix

$$\begin{pmatrix} p'_0 & 0 & 0 & 0 & r'_0 \\ p'_1 & p'_0 & 0 & 0 & r'_1 \\ p'_2 & p'_1 & p'_0 & 0 & r'_2 \\ p'_3 & p'_2 & p'_1 & p'_0 & r'_3 \\ 0 & 0 & 0 & 0 & g'_0 \\ c'_1 & 0 & 0 & 0 & g'_1 \\ c'_2 & c'_1 & 0 & 0 & g'_2 \\ c'_3 & c'_2 & c'_1 & 0 & g'_3 \end{pmatrix}.$$

Note that we need no additional computations to generate these new entries: Due to the Topelitz structure of our matrix the (4, 8)-plane rotation has already generated all the necessary numbers. Thus, the whole process up to this point requires only  $O(n)$  operations.

We now generate a rotation in the (3, 8)-plane to annihilate  $c'_1$ . This gives the matrix

$$\begin{pmatrix} p'_0 & 0 & 0 & 0 & r'_0 \\ p'_1 & p'_0 & 0 & 0 & r'_1 \\ p''_2 & p''_1 & p''_0 & 0 & r''_2 \\ p'_3 & p'_2 & p'_1 & p'_0 & r'_3 \\ 0 & 0 & 0 & 0 & g'_0 \\ c'_1 & 0 & 0 & 0 & g'_1 \\ c'_2 & c'_1 & 0 & 0 & g'_2 \\ c''_3 & c''_2 & 0 & 0 & g''_3 \end{pmatrix}.$$

If this rotation is applied in the (2, 7)- and (1, 6)-planes, the result is

$$\begin{pmatrix} p_0'' & 0 & 0 & 0 & r_0'' \\ p_1'' & p_0'' & 0 & 0 & r_1'' \\ p_2'' & p_1'' & p_0'' & 0 & r_2'' \\ p_3' & p_2' & p_1' & p_0' & r_3' \\ 0 & 0 & 0 & 0 & g_0'' \\ 0 & 0 & 0 & 0 & g_1'' \\ c_2' & 0 & 0 & 0 & g_2'' \\ c_3'' & c_2'' & 0 & 0 & g_3'' \end{pmatrix}.$$

Once again the time consumed is  $O(n)$ .

Continuing in this manner we get

$$\begin{pmatrix} p_0''' & 0 & 0 & 0 & r_0''' \\ p_1''' & p_0''' & 0 & 0 & r_1''' \\ p_2'' & p_1'' & p_0'' & 0 & r_2'' \\ p_3' & p_2' & p_1' & p_0' & r_3' \\ 0 & 0 & 0 & 0 & g_0'' \\ 0 & 0 & 0 & 0 & g_1'' \\ 0 & 0 & 0 & 0 & g_2''' \\ c_3'' & 0 & 0 & 0 & g_3''' \end{pmatrix},$$

and finally

$$\begin{pmatrix} p_0'''' & 0 & 0 & 0 & r_0'''' \\ p_1'''' & p_0'''' & 0 & 0 & r_1'''' \\ p_2'' & p_1'' & p_0'' & 0 & r_2'' \\ p_3' & p_2' & p_1' & p_0' & r_3' \\ 0 & 0 & 0 & 0 & g_0'' \\ 0 & 0 & 0 & 0 & g_1'' \\ 0 & 0 & 0 & 0 & g_2'''' \\ 0 & 0 & 0 & 0 & g_3'''' \end{pmatrix} \equiv \begin{pmatrix} \ell_{00} & 0 & 0 & 0 & u_0 \\ \ell_{10} & \ell_{11} & 0 & 0 & u_1 \\ \ell_{20} & \ell_{21} & \ell_{22} & 0 & u_2 \\ \ell_{30} & \ell_{31} & \ell_{32} & \ell_{33} & u_3 \\ 0 & 0 & 0 & 0 & g_0 \\ 0 & 0 & 0 & 0 & g_1 \\ 0 & 0 & 0 & 0 & g_2 \\ 0 & 0 & 0 & 0 & g_3 \end{pmatrix},$$

which completes the reduction. Since each stage requires at most  $O(n)$  work and there are  $n$  stages, the algorithm as a whole requires  $O(n^2)$  work.

The input to the algorithm are the vectors  $p$ ,  $r$ , and  $c$ . The output is the matrix  $L$  and the vector  $u$ . The former is not Toeplitz and must be stored explicitly, making the storage requirement for the algorithm  $O(n^2)$ .

## 4 Results

In what follows we discuss a number of problems concerning short range acoustic propagation in shallow water. The stratified environment consists of a rigid bottom and two propagation media, namely a 100-meter column of water with slowly varying sound speed profile and a 20-meter sub-bottom with a constant sound speed profile. The interfaces have zero roughness. All the receiver and source series were generated using the Fast Field Program [15]. The first derivative constraint for the Tikhonov–Philips regularization of the problems was used throughout.

It is important to recall at this point that, in accordance with the discussion in the Introduction section, the ill-conditionness of the propagation operator is not simply a consequence of a chosen sampling rate, but is rather an inherent problem in underwater acoustics. As far as the success of the deconvolution technique is concerned, what is important is that our time domain sampling rate be such that the variation of the source function on that scale be relatively slow. For a person used to working in the frequency domain, the latter statement can be translated into a requirement that the frequency content of the source in the vicinity of the Nyquist frequency be small compared to the rest of the spectrum. In other words, a good performance of the deconvolution method is expected only if the source function is oversampled in time. In what follows, by "high frequencies" we will mean those frequencies that are in "relatively close" proximity to the Nyquist frequency.

As was mentioned earlier, the Fast Field Program takes advantage of the horizontal stratification and performs direct time-domain broad band computations. The time domain discretization is accomplished using the finite element method [3].

Consider a situation with a source placed at a depth of 15 meters and a receiver at a range of 100 meters from the source and a depth of 25 meters. The environment is as described earlier. Figure 2a is the time domain plot of the impulse response generated by the Fast Field Program and Figure 2b is the modulus of its Discrete Fourier Transform (DFT). It is this response that represents the discretized version of the kernel function and is the sole carrier of the ill-conditionness of the corresponding matrix operator.

It seems natural to start our numerical examples with a case where the actual source is a pulse. Figures 3 and 3b represent a broadband source (the object of the deconvolution process) and the modulus of its DFT. For the sake of simplicity we refer to this source as G-source. From the relatively flat shape of the Fourier

transform one can see that in the time domain the source is close to the Kronecker delta, whose spectrum is constant. This spiked source function is a challenge as far as its deconvolution using Tikhonov–Phillips regularization is concerned. This is due to the fact that the regularization imposes a smoothness constraint, which could be at odds with the shape of a function like G-source.

A windowed response to G-source and the modulus of its DFT are displayed on figures 4a and 4b. Because the source function is extremely narrow in the time domain its responses in the time and frequency domains are quite similar in shape to those of the impulse response of Figs. 2a and b.

We use the normwise relative error

$$\frac{\|x - y\|}{\|x\|}$$

as a measure of the dissimilarity in the vectors  $x$  and  $y$ . It should be stressed, that this measure is pessimistic, especially in cases where the source is zero except over a small interval. Generally the reconstructed signal tracks the features of the original better than might be expected from the relative error. However, the measure serves to define the interval in which the regularization parameter is giving reasonable results. Perhaps a norm defined using an ad hoc inner product matrix that emphasizes the larger absolute values of the deconvolved functions would serve a more useful relative error description.

Figure 5 is a plot of the common logarithm of relative error as a function of  $\lambda/h$  pertaining to the source deconvolution process.  $STSactl$  and  $STSsrcvd$  refer to the actual and deconvolved source time series respectively. One can see that although the range of values for  $\lambda/h$  yielding relative errors below 0.36 (i.e.,  $\text{Log}_{10}(\text{relative error}) \leq -0.5$ ) is quite wide, the values never fall below 0.16 ( $\text{Log}_{10}(\text{relative error}) \leq -0.8$ ).

The high relative error is to be expected in a problem which has been chosen to be unsmooth — that is one in which high frequency components are important. As we suggested above, however, the visual agreement of the reconstructed signal and the original is quite good. Figures 6a and 6b are a plot of the deconvolved G-source and a zoom-in on its central portion obtained by using the value of  $\lambda/h$  corresponding to the minimum of the relative error of Fig. 5. It is seen that the deconvolved signal reproduces the magnitude and location of the pulse quite accurately.

To see how smoothness affects the reconstruction we applied the deconvolution process to a somewhat smoother function, which we call C-source. Figures 7a, 7b

and time and frequency series for C-source and its response correspondingly. We can observe that the high frequency content in this case is significantly reduced in both the source and the receiver series compared to the previous case. From Fig. 9 we see that the minimum values attained by the relative error are also noticeably smaller compared to the previous case.

A number of deconvolutions were performed for the values of  $\text{Log}_{10}(\lambda/h)$  from the interval of  $(-6.5, -4.5)$ . Figure 10 is a typical outcome of the deconvolution in that region. The visual agreement between the actual source and the deconvolved one in this case is excellent.

To look at the influence of white noise on the deconvolution process the latter was added to the receiver series prior to the deconvolution. Figure 11 is a plot of the relative error as a function of  $\text{Log}_{10}(\lambda/h)$  for the case of signal-to-white-noise ratio of the integrated field intensities of 0dB. We can see that at this level of white noise the relative error never comes close to the low values obtained in the noiseless case. In fact, the lowest value obtained here is approximately  $10^{-0.4} = 0.40$ . Nevertheless, the relative error stays flat near its minimum for the values of  $\text{Log}_{10}(\lambda/h)$  ranging over close to two orders of magnitude. Figure 12 is a plot of the recovered C-source corresponding to  $\text{Log}_{10}(\lambda/h)$  at the minimum of the previous plot. Once again the location of the peak and its shape are matched quite well.

We proceed by repeating the above study for two cases of source functions that are broadband but not of a pulse type. In addition we slightly alter the source-receiver geometry. At this time the source and receiver are both at the depth of 10 meters and are 100 meters apart.

Figures 13a and 13b are the impulse response and the modulus of its DFT for the current source-receiver configuration. Figures 14a and 14b and 15a, 15b represent the time and frequency series for H-source and its response correspondingly. It is easy to see that both are relatively broadband. Just as before, we obtain a curve of the dependence of the relative error on  $\lambda/h$ , which is displayed in Fig. 16. From this figure we observe that the lowest values of the relative error are somewhat shallow, as was the case for G-source. We also see that the range of values of  $\lambda/h$  for which the measure is close to its minimum is rather small. We argue again that this discrepancy is caused by the fact that the relative weight of the high frequency components is relatively high for H-source, similar to the situation for G-source (Fig. 4b).

Using the value of  $\lambda/h$  corresponding to the minimum of the relative error we perform the deconvolution and obtain Figs. 17a, 17b, and 17c, which represent

the three consecutive segments of the windowed source function. We see that the agreement between the actual source and the deconvolved one is quite good initially, but deteriorates toward the end.

Next we repeat the computations for a source that is not quite as broadband. Figures 18a, 18b and and frequency series for I-source and its response correspondingly. It is obvious that the highest frequencies for this source and its response are not as prominent as those for the previous source and its response.

Figure 20 for the variation of the relative error as a function of  $\text{Log}(\lambda/h)$  seems to again suggest that going with smoother source functions leads to improved deconvolution results over a wide range of values of  $\lambda/h$ . The plot of the deconvolved series for the value of  $\text{Log}(\lambda/h)$  corresponding to the minimum of the previous plot is displayed on Figs. 21a, 21b, 21c. One can see that in this case the agreement between the actual source and the recovered one is excellent.

Finally, we apply white noise to the receiver series generated by I-source prior to the deconvolution. While the deconvolution results for 0.0dB signal-to-white-noise ratio of the integrated intensities were acceptable, they were not as impressive as those for C-source with the same noise ratio. Therefore we increased the ratio in this example to 6.0dB. Figure 22 is a plot of the relative error for this case. One can see here that the range of  $\lambda/h$  values for which the relative error is less than unity is over two orders in magnitude and is practically the same as that for C-source deconvolution and 0dB signal-to-white-noise ratio of the integrated intensities. Figures 23a, 23b, and 23c give the portions of the deconvolved series for the case of the lowest relative error. Again, the agreement between the actual source series and the deconvolved one seems quite noticeable.

## 5 CONCLUSIONS AND FUTURE WORK

We have demonstrated how Tikhonov–Phillips regularization can be applied to the deconvolution of an acoustic source for a simple shallow water environment. The advantage of this method of deconvolution over those performed in the frequency domain is twofold. First in problems requiring numerous deconvolutions of broadband signals in multipath environments, i.e. those environments where the signal does not rapidly die off, computational effort can be saved by working with smaller windows. Second, the fact that the matrix of the discrete problem is triangular and Toeplitz allows us to use Eldén’s algorithm to reduce the computations by a factor of  $n$ .

The deconvolution results are better when the high frequency components of the source, i.e. the content of the frequencies in the vicinity of the Nyquist

frequency, are smaller than the components at the lower frequencies.

The sensitivity of the method to the variation of the regularization parameter was tested in a number of examples. We found that in our applications the method was robust for a relatively wide range of the parameter values, even in the presence of a substantial amount of white noise.

It will be interesting in the future to test the deconvolution procedure in the presence of noise that is not white. Of particular interest to us is the situation where the deconvolution has to be performed in the presence of the signal due to the part of the source signal that occurred prior to its current windowed portion.

## 6 Acknowledgements

The authors would like to express their gratitude to Michael Porter of NJIT for the numerous consultations on his Fast Field Program. Our thanks also go to John Perkins of NRL for his effort in reviewing the manuscript. Part of this work was supported by the National Science Foundation under Grant CCR9503126.

## References

- [1] R. S. Andersen, F. R. De Hoog, and M. A. Lukas, editors. *The Application and Numerical Solution of Integral Equations*. Sijthoff and Noordhoff, Alphen aan den Rijn, Netherlands, 1980.
- [2] E. Anderson, Z. Bai, C. Bischof, J. Demmel, J. Dongarra, J. Du Croz, A. Greenbaum, S. Hammarling, A. McKenney, S. Ostrouchov, and D. Sorensen. *LAPACK Users' Guide*. SIAM, Philadelphia, second edition, 1995.
- [3] E. B. Becker, G. F. Carey, and J. T. Oden. *Finite Elements: An Introduction*. Prentice-Hall, Englewood Cliffs, NJ, 1981.
- [4] C. A. Berenstein and E. V. Patrick. Exact deconvolution for multiple convolution operators—an overview, plus performance characterizations for imaging sensors. *Proceedings of the IEEE*, 78:723–734, 1990.
- [5] J. V. Candy, R. W. Ziolkowski, and D.K.Lewis. Transient wave estimation: A multichannel deconvolution application. *Journal of the Acoustical Society of America*, 88:2235–2247, 1990.

- [6] E. B. Davies and E. J. Mercado. Multichannel deconvolution filtering of field recorded seismic data. *Geophysics*, 33:711–722, 1968.
- [7] P. Deuffhard and E. Hairer, editors. *Numerical Treatment of Inverse Problems in Differential and Integral Equations*. Birkhäuser, Boston, 1983.
- [8] R. L. Dicus. Impulse response estimation with underwater explosive charge acoustic signals. *J. Acoustic. Soc. Am.*, 70:122–133, 1981.
- [9] L. Eldén. An efficient algorithm for the regularization of ill-conditioned least squares problems with a triangular Toeplitz matrix. *SIAM Journal on Scientific and Statistical Computing*, 5:229–236, 1984.
- [10] M. Hanke and P. C. Hansen. Regularization methods for large-scale problems. *Surveys on Mathematics for Industry*, 3:253–315, 1993.
- [11] P. C. Mignerey and S. Finette. Multichannel deconvolution of an acoustic transient in an oceanic waveguide. *Journal of the Acoustical Society of America*, 92:351–364, 1992.
- [12] P. C. Mignerey, S. Finette, and J. F. Smith III. Broadband source signature extraction using a vertical array. *Journal of the Acoustical Society of America*, 94:309–318, 1993.
- [13] D. P. O’Leary and J. A. Simmons. A bidiagonalization-regularization procedure for large scale discretizations of ill-posed problems. *SIAM Journal on Scientific and Statistical Computing*, 2:474–489, 1981.
- [14] D. L. Phillips. A technique for the numerical solution of certain integral equations of the first kind. *Journal of the ACM*, 87:84–96, 1962.
- [15] M. B. Porter. The time-marched fast-field program (ffp) for modeling acoustic pulse propagation. *Journal of the Acoustical Society of America*, 87:2013–2023, 1990.
- [16] W. W. Schmaedeke. Approximate solutions for volterra integral equations of the first kind. *Journal of Mathematical Analysis and Applications*, 23:604–613, 1968.
- [17] A. N. Tikhonov and V. Y. Arsenin. *Solutions of Ill-Posed Problems*. Winston and Sons, Washington, DC, 1977.



- [18] G. M. Webster, editor. *Deconvolution, Vol. I,II*. Society of Exploration Geophysics, Tulsa, 1978. In Geophysics Reprints Series No. 1.

Figure 1: This (missing) figure illustrates how the particular choice of correspondence between the elements of windowed source and receiver time series results in a lower triangular Toeplitz matrix.

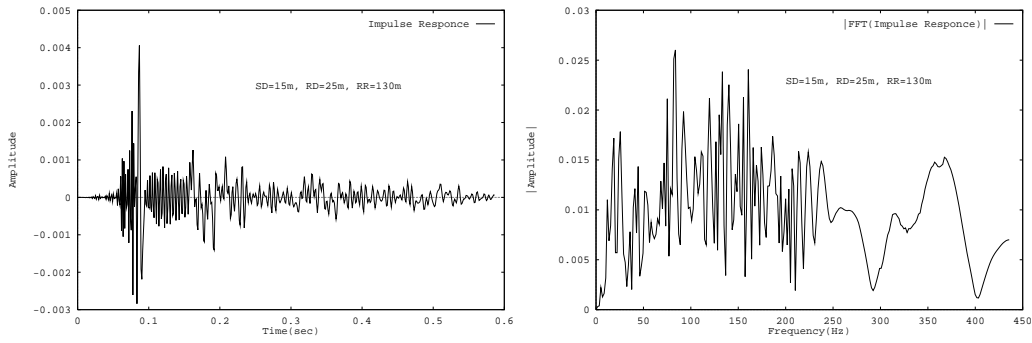


Figure 2: a) Time-domain impulse response. b) Absolute value of the DFT of the time-domain impulse response.

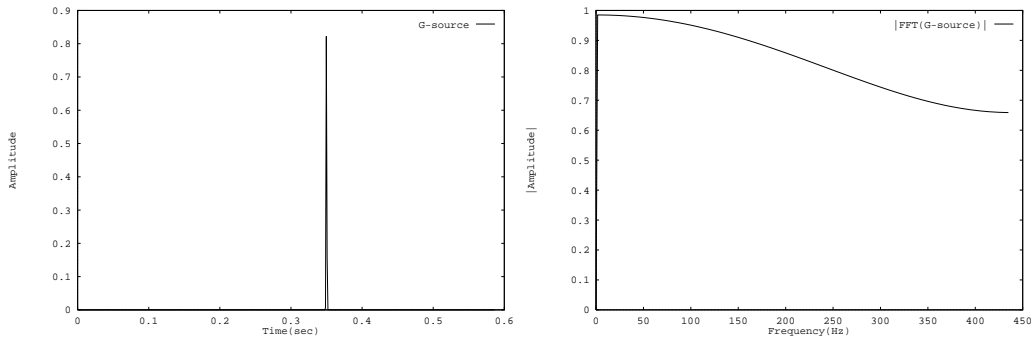


Figure 3: a) G-source time series. b) Absolute value of the DFT of G-source time series.

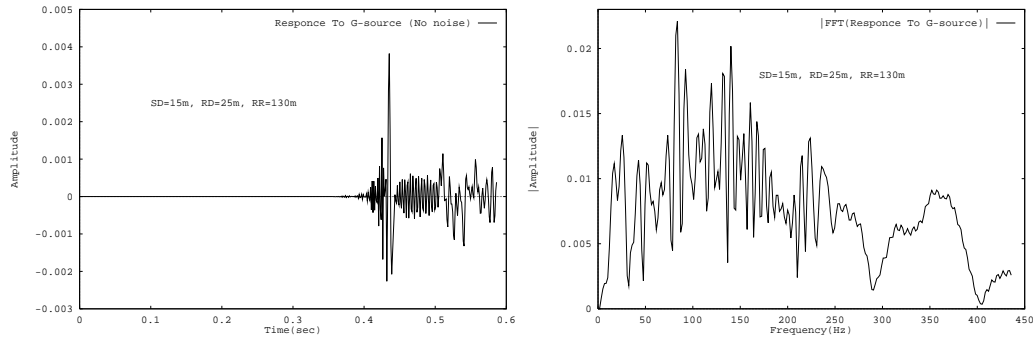


Figure 4: a) Time-domain response to G-source. b) Absolute value of the DFT of the time-domain response to G-source.

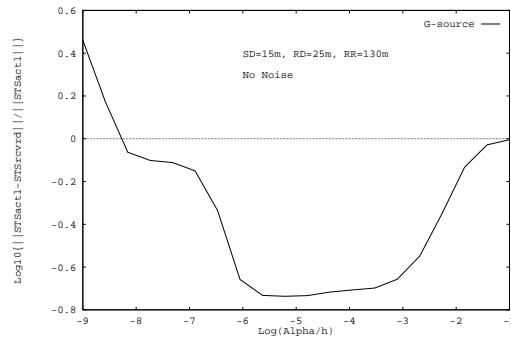


Figure 5: Variation of the relative for deconvolution of G-source in the absence of noise.

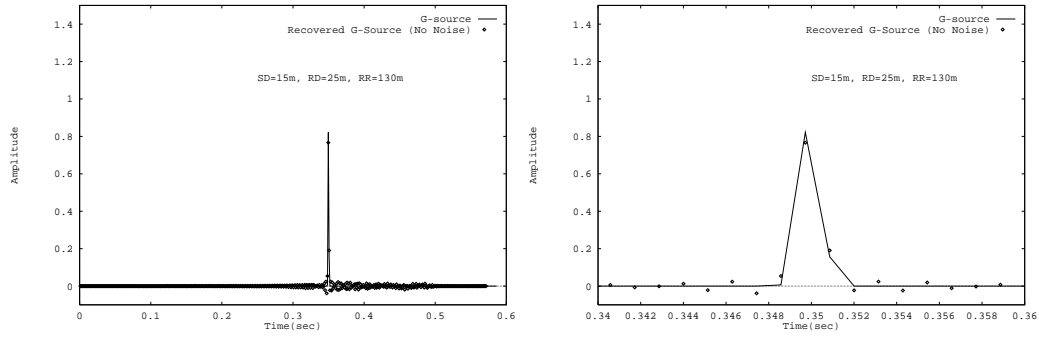


Figure 6: a) Deconvolution of G-source in the absence of noise. b) Zoom-in on the central portion of the deconvolved G-source.

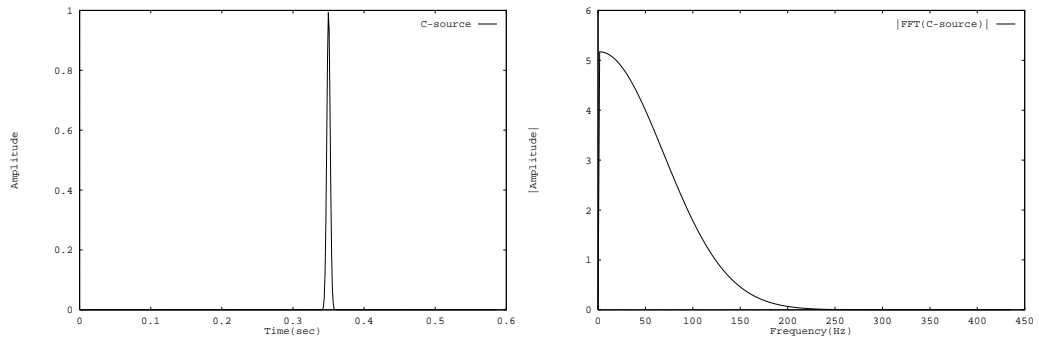


Figure 7: a) C-source time series. b) Absolute value of the DFT of C-source time series.

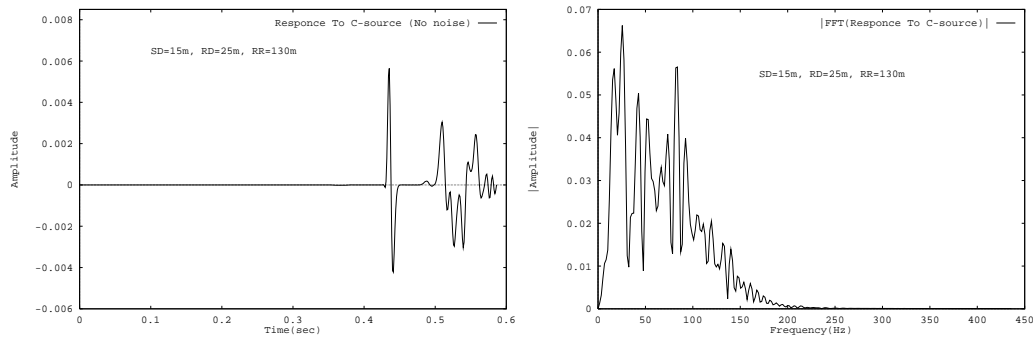


Figure 8: a) Time-domain response to C-source. b) Absolute value of the DFT of the time-domain response to C-source.

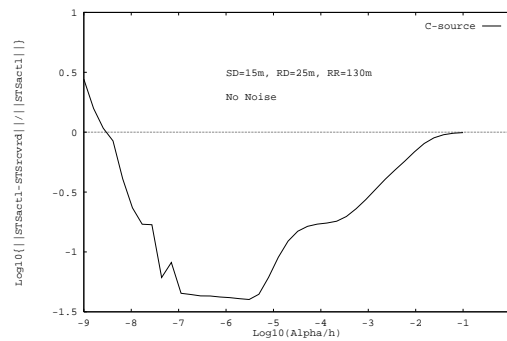


Figure 9: Variation of the relative error for deconvolution of C-source in the absence of noise.

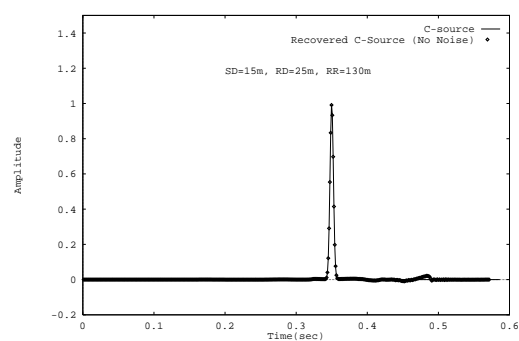


Figure 10: Deconvolution of C-source in the absence of noise.

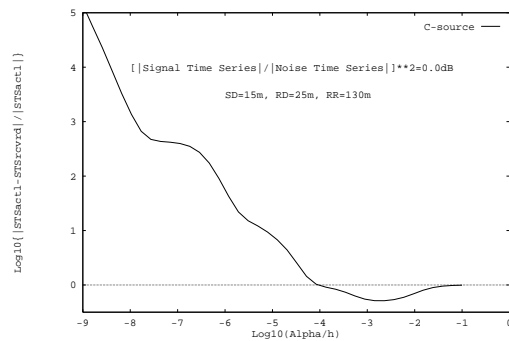


Figure 11: Variation of the relative error for deconvolution of C-source in the presence of  $\left[\frac{\|\text{signal}\|}{\|\text{white noise}\|}\right]^2=0.0\text{dB}$  on the receiver.

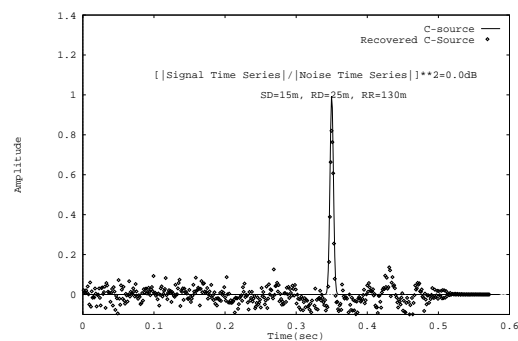


Figure 12: C-source deconvolution in the presence of  $\left[\frac{\|\text{signal}\|}{\|\text{white noise}\|}\right]^2 = 0.0\text{dB}$  on the receiver.

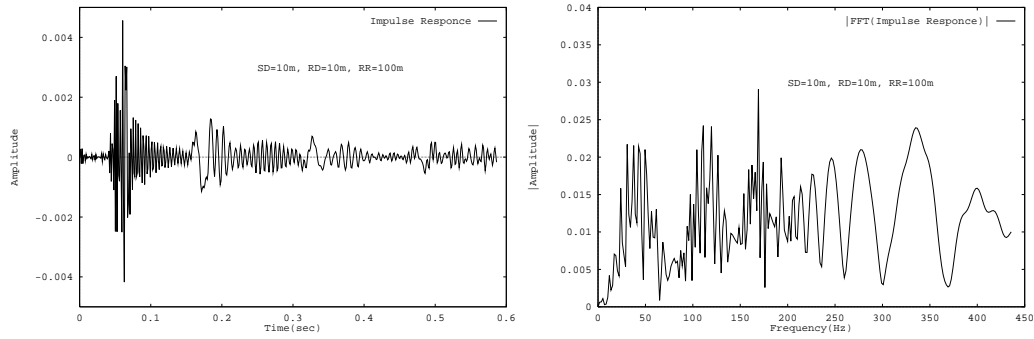


Figure 13: a) Time-domain impulse response. b) Absolute value of the DFT of the time-domain impulse response.

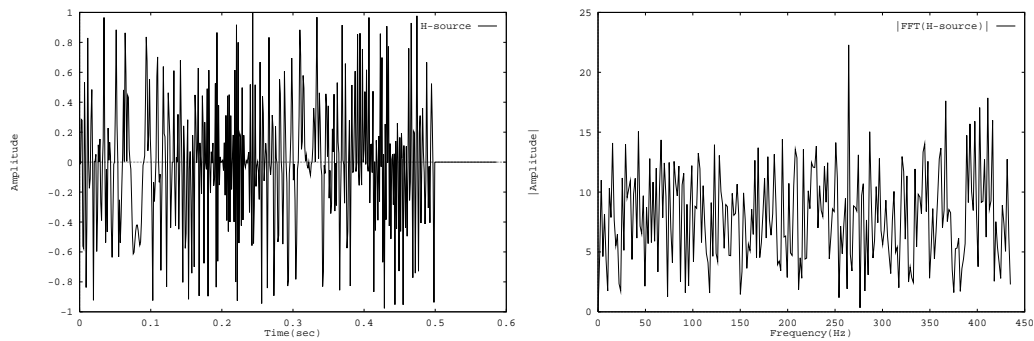


Figure 14: a) H-source time series. b) Absolute value of the DFT of H-source time series



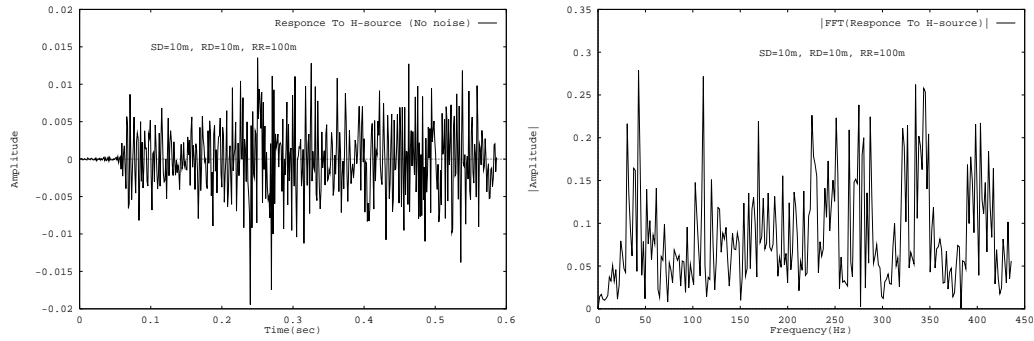


Figure 15: a) Time-domain response to H-source. b) Absolute value of the DFT of the time-domain response to H-source.

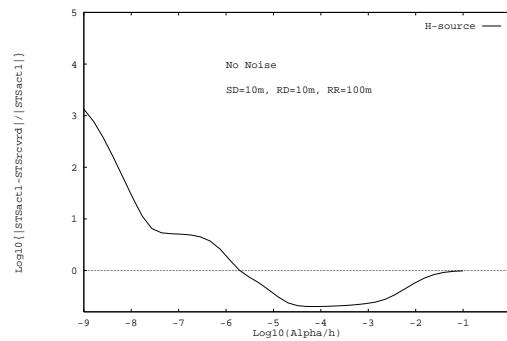


Figure 16: Variation of the dissimilarity measure for deconvolution of H-source in the absence of noise.

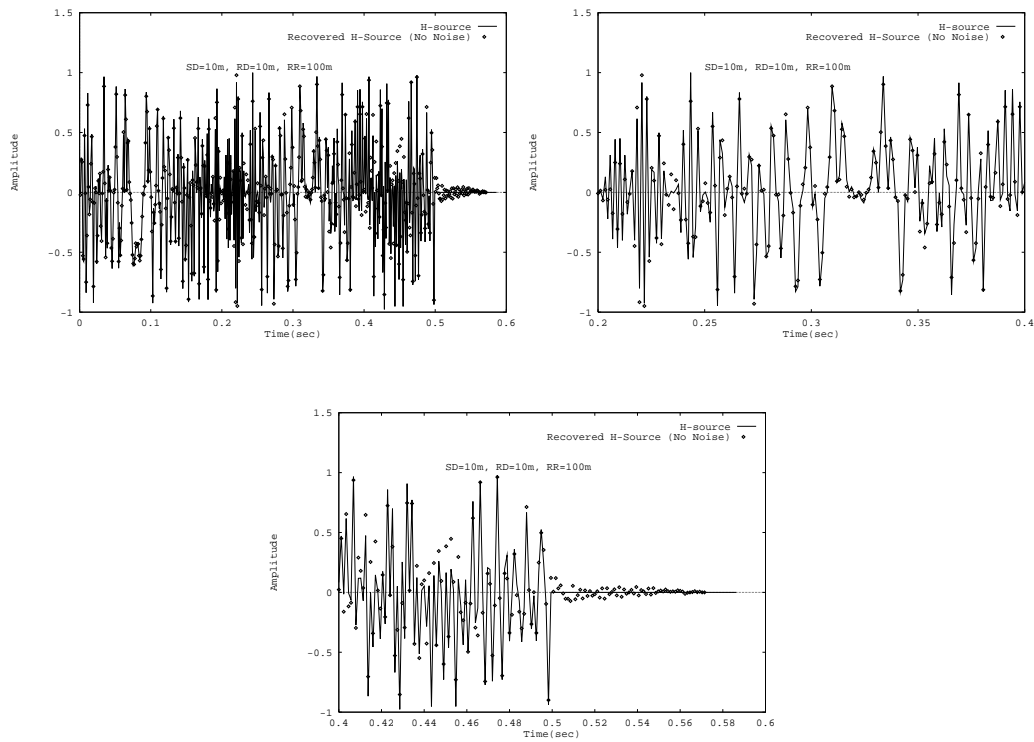


Figure 17: a),b),c) - the portions of the deconvolved H-source in the absence of noise.

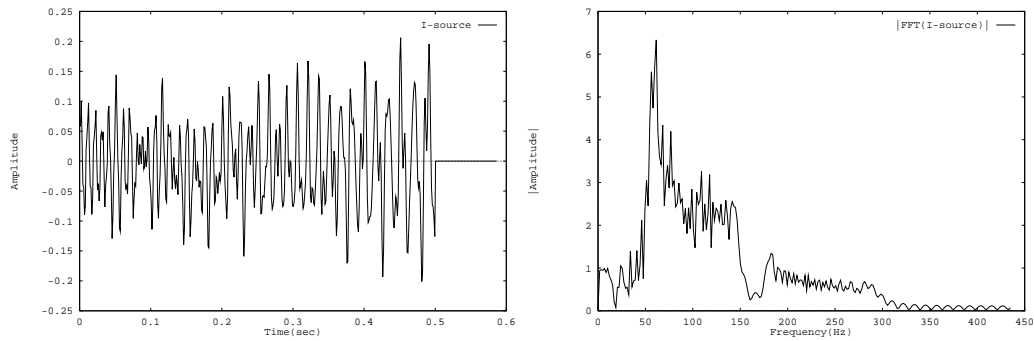


Figure 18: a) I-source time series. b) Absolute value of the DFT of I-source time series.

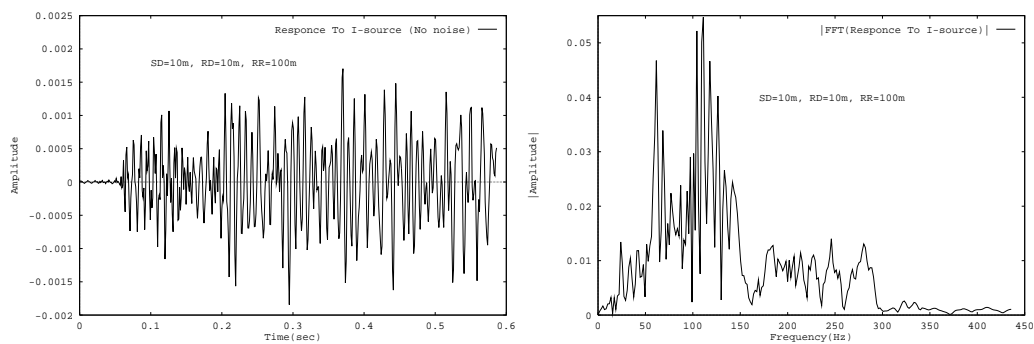


Figure 19: a) Time-domain response to I-source. b) Absolute value of the DFT of the time-domain response to I-source.

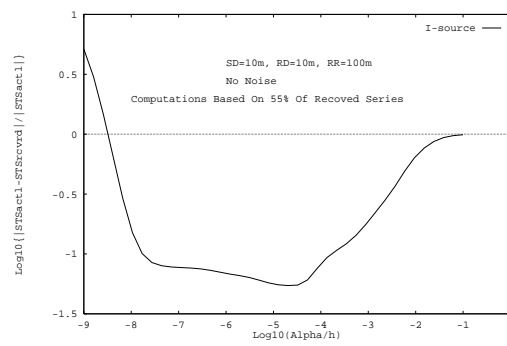


Figure 20: Variation of the relative error for deconvolution of I-source in the absence of noise.

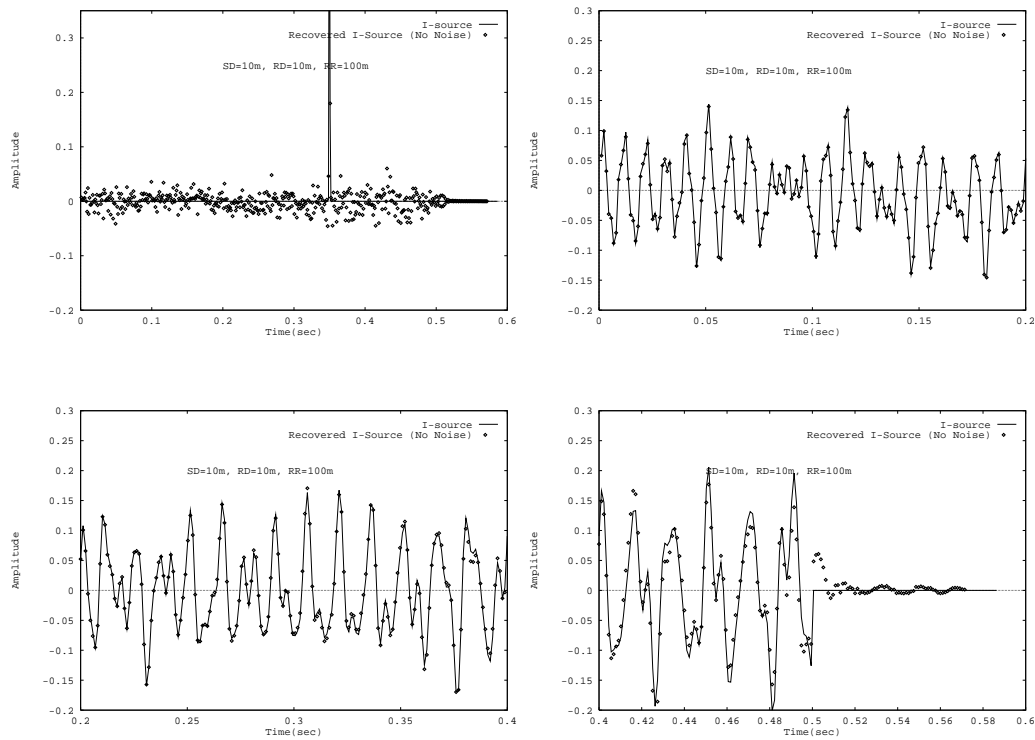


Figure 21: a),b),c) - the portions of the deconvolved I-source in the absence of noise.

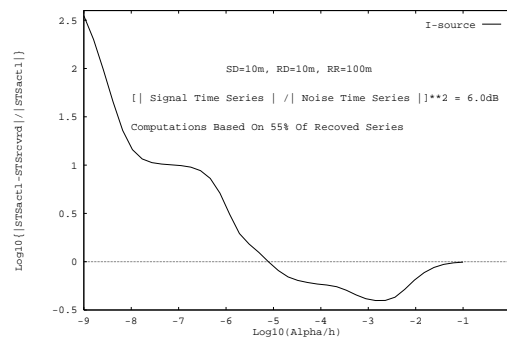


Figure 22: Variation of the relative error for deconvolution of I-source in the presence of  $(\| \text{signal} \| / \| \text{white noise} \|^2 = 6.0\text{dB})$  on the receiver.

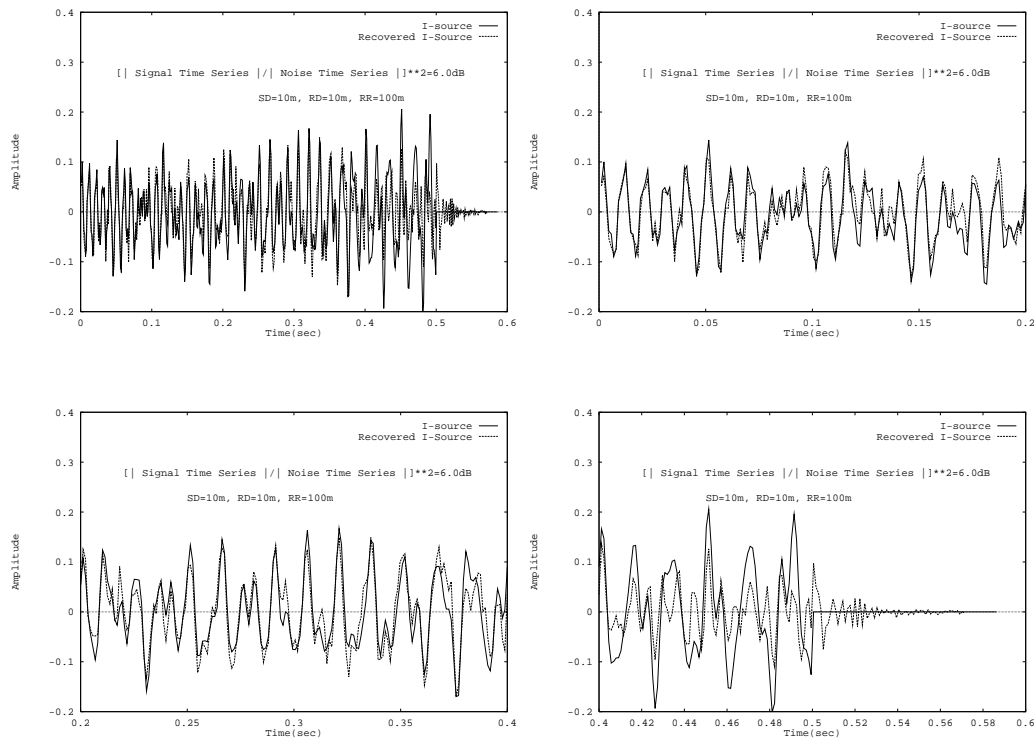


Figure 23: a), b), c) - The three segments of the deconvolved I-source in the presence of  $\left[\frac{\| \text{signal} \|}{\| \text{white noise} \|}\right]^2 = 6.0\text{dB}$  on the receiver.